



## Original Research Article

T7 RNA polymerase-guided base editor for accelerated continuous evolution in *Bacillus subtilis*

Bin Wang<sup>a,b,c</sup>, Yaokang Wu<sup>a,b,c</sup> , Xueqin Lv<sup>a,b,c</sup>, Long Liu<sup>a,b,c</sup>,  
Jianghua Li<sup>b,c</sup>, Guocheng Du<sup>a,b,c</sup>, Jian Chen<sup>b,c</sup>, Yanfeng Liu<sup>a,b,c,\*</sup> 

<sup>a</sup> School of Biotechnology and Key Laboratory of Carbohydrate Chemistry and Biotechnology, Ministry of Education, School of Biotechnology, Jiangnan University, Wuxi, 214122, China

<sup>b</sup> Science Center for Future Foods, Jiangnan University, Wuxi, 214122, China

<sup>c</sup> Jiangsu Province Basic Research Center for Synthetic Biology, Jiangnan University, Wuxi, 214122, China



## ARTICLE INFO

## Keywords:

T7 RNA polymerase  
Continuous directed evolution  
BS-MutaT7 system  
*Bacillus subtilis*

## ABSTRACT

Targeted *in vivo* hypermutation mediated by base deaminase-T7 RNA polymerase (T7 RNAP) fusions promotes genetic diversification and accelerates continuous directed evolution. Due to the lack of a T7RNAP expression regulation system and functionally compatible linker for fusion protein expression, T7RNAP-guided continuous evolution has not been established in *Bacillus subtilis*, which limited long gene fragment continuous evolution targeted on genome. Here, we developed BS-MutaT7 system, which introduced mutations into specific genomic regions by leveraging chimeric fusions of base deaminases with T7RNAP in *B. subtilis*. We selected seven different sources of adenosine and cytosine deaminases, 14 fusion protein linkers to be fused with T7RNAP, constructing four libraries with the size of 5000, where deaminases were fused at either the N- or C-terminus of T7RNAP. Based on the efficiency of binding to T7 promoter and high mutagenesis activity, two optimal chimeric mutators, BS-MutaT7<sup>A</sup> (TadA8e-Linker0-T7RNAP) and BS-MutaT7<sup>C</sup> (PmCDA1-(GGGS)<sub>3</sub>-T7RNAP co-expressed with UGI) were identified. The target mutation rates reached  $1.2 \times 10^{-5}$  per base per generation (s.p.b.) and  $5.8 \times 10^{-5}$  s.p.b., representing 7000-fold and 37,000-fold increases over the genomic mutation rate, respectively. Both exhibited high processivity, maintaining mutation rates of  $5.8 \times 10^{-6}$  s.p.b. and  $2.9 \times 10^{-5}$  s.p.b. within a 5 kb DNA region. Notably, BS-MutaT7<sup>C</sup> exhibited superior mutagenic activity, making it well-suited for applications requiring intensive and sustained genomic diversification. Application of BS-MutaT7 enabled a 16-fold increase in tigecycline resistance and enhanced  $\beta$ -lactoglobulin ( $\beta$ -Lg) expression by evolving the global transcriptional regulator *codY*, achieving a  $\beta$ -Lg titer of 3.92 g/L. These results highlight BS-MutaT7 as a powerful and versatile tool for genome-scale continuous evolution in *B. subtilis*.

## 1. Introduction

Directed evolution offers a rational and versatile strategy for enhancing protein function by emulating natural selection in the laboratory. Through iterative cycles of mutation and screening, it has driven significant progress in enzyme engineering, therapeutics, and synthetic biology [1–3]. However, traditional *in vitro* protein evolution strategies are constrained by low transformation efficiency, prolonged evolution time, poor mutant adaptability, and discontinuous workflows [4,5]. These challenges have recently been overcome by continuous directed

evolution (CDE), which utilizes *in vivo* hypermutation to enable continuous mutagenesis under natural physiological conditions. This approach allows the direct selection of functional mutants, significantly accelerating *in situ* protein evolution [6–8]. Moreover, *in vivo* hypermutation approach can specifically introduce mutations into the target gene, minimizing harm to host cells.

Based on distinct mechanisms and mutation-targeted regions, various methods for targeted *in vivo* protein evolution have been developed. For instance, virus-based phage-assisted continuous evolution (PACE) can induce mutations across the entire genome [9], while

Peer review under the responsibility of Editorial Board of Synthetic and Systems Biotechnology.

\* Corresponding author. School of Biotechnology and Key Laboratory of Carbohydrate Chemistry and Biotechnology, Ministry of Education, School of Biotechnology, Jiangnan University, Wuxi, 214122, China

E-mail address: [yanfengliu@jiangnan.edu.cn](mailto:yanfengliu@jiangnan.edu.cn) (Y. Liu).

<https://doi.org/10.1016/j.synbio.2025.04.010>

Received 4 March 2025; Received in revised form 29 March 2025; Accepted 19 April 2025

Available online 21 April 2025

2405-805X/© 2025 The Authors. Publishing services by Elsevier B.V. on behalf of KeAi Communications Co. Ltd. This is an open access article under the CC BY-NC-ND license (<http://creativecommons.org/licenses/by-nc-nd/4.0/>).

the orthogonal DNA polymerase-based evolution systems introduce mutations specifically on plasmids using an orthogonal error-prone DNA polymerase [10–12]. CRISPR-based targeted evolution systems, such as EvolvR [13], base editors (BE) [13–20], and prime editors [21,22], generate mutations have been developed. The EvolvR system fused nCas9 with a nick-translating and error-prone DNA polymerase to create nicks on double-stranded DNA and introduces mismatches [13]. The base editors were created by fusing cytosine deaminase or adenine deaminase to the dCas9 or nCas9 to introduce mutations in the genomic target. The prime editing system consisted of a catalytically impaired Cas9 fused to an engineered reverse transcriptase and a prime editing guide RNA (pegRNA), which identified the target site and encoded the target DNA nucleotides [21,22]. However, these systems introduced the mutations in a small region of the gene. To expand this window, orthogonal T7 RNA polymerase (T7RNAP)-based evolution systems have been developed by fusing base deaminases (BD) with T7RNAP. The cytosine deaminases (CD) introduce C > T and G > A substitutions and engineered adenosine deaminases (AD) introduce A > G and T > C substitutions. The BD-T7RNAP exploits the specificity of T7RNAP for the T7 promoter (P<sub>T7</sub>) to precisely locate the target DNA region, where deaminase introduces mutations [23]. To broaden mutation spectrum, a dual gene-specific mutator system combining CD and AD with T7RNAP has been constructed, enabling more variations [24]. Additionally, by positioning P<sub>T7</sub> appropriately, mutations can be introduced on the coding strand, the non-coding strand, or both simultaneously [25,26]. This system has been effectively applied across various organisms, including *Escherichia coli* (eMutaT7) [24–29], yeast (TRIDENT) [30], *Corynebacterium glutamicum* (CgMutaT7) [31], plants [32], and mammalian cells (TRACE) [33]. In *E. coli*, the eMutaT7<sup>PmCDA1</sup> system achieved a mutation rate of  $9.4 \times 10^{-5}$  per base per generation within a ~1 kb target region [26], while the later-developed eMutaT7<sup>TadA-8e</sup> system showed 2.4-fold lower efficiency [24]. Similarly, Cravens et al. demonstrated the broad applicability of CD-T7RNAP and AD-T7RNAP systems in *S. cerevisiae* [30]. These findings underscore the BD-T7RNAP system as a versatile and powerful tool for in vivo protein evolution via in situ mutagenesis.

Currently, continuous evolution strategies are focused on the CRISPR-based targeted system and the T7RNAP-guided evolution system has not yet been established in *B. subtilis*. The CRISPR-based targeted systems were developed by fusing cytosine deaminase, adenosine deaminase with nCas9, Cas12b, and dCas12a, which operate in a discontinuous manner and are constrained to narrow genomic windows [18–20,34]. It is necessary to design multiple gRNAs or crRNAs when mutating long gene fragment and operons. The BD-T7RNAP system with high processivity circumvents these limitations by enabling continuous mutagenesis in target regions under the control of T7 promoter. However, the application of T7RNAP in *B. subtilis* remains constrained by the absence of a well-defined regulatory system, which is essential for mutagenesis-driven evolution, as unregulated expression may cause cellular toxicity and impair growth. In addition, the fusion protein linker critically influences protein expression and screening for functionally compatible linker is essential for achieving high-level expression.

In this study, we developed a deaminase-T7RNAP-based evolution system in *B. subtilis* (BS-MutaT7) for targeted *in situ* mutagenesis. First of all, seven different sources of adenosine and cytosine deaminases, along with 14 fusion protein linkers were selected, and constructed four libraries with deaminases fused at either the N- or C-terminus of T7RNAP. Based on the efficiency of binding to T7 promoter and high mutagenesis activity, two optimal single-base editor systems: BS-MutaT7<sup>A</sup> (TadA8e-Linker0-T7RNAP) and BS-MutaT7<sup>C</sup> (PmCDA1-Linker5-T7RNAP co-expressed with UGI) were identified. Subsequently, we verified the sustained mutagenic activity of BS-MutaT7 system within a 5 kb DNA region. Finally, the BS-MutaT7 system was applied to the continuous evolution of the tetracycline efflux transporter TetK, enhancing the tigecycline tolerance in *B. subtilis*. These findings demonstrate the potential of BS-MutaT7 as a powerful platform for high-efficiency,

processive evolution, broadening the scope of continuous directed evolution in prokaryotic cell.

## 2. Materials and methods

### 2.1. Chemicals and reagents

Unless specified otherwise, all chemicals and reagents were purchased from Sangon Biotech (Shanghai, China). Tigecycline standard was purchased from Sigma-Aldrich (Shanghai, China). DNA gel purification kit was obtained from Thermo Scientific (Waltham, USA). PrimeSTAR® Max DNA polymerase and Rapid Taq Master Mix were purchased from Takara Biomedical Technology (Beijing, China) and Vazyme Biotech Co., Ltd. (Nanjing, China), respectively. The Seamless Cloning Kit for plasmid and library construction was supplied by Vazyme Biotech Co., Ltd. (Nanjing, China). Oligonucleotides were synthesized by GENEWIZ (Suzhou, China).

### 2.2. Strains, medium and cultivation conditions

All strains used in this study are listed in Table 1. The *E. coli* JM110 was used for plasmid construction and *B. subtilis* 168 served as the initial host strain. Genome editing in *B. subtilis* was conducted using the Cre/lox system and PCR-based genome engineering approach [35]. *B. subtilis* were transformed into super-competent cells using a previously described protocol [36]. Both *E. coli* and *B. subtilis* strains were cultured in Luria-Bertani (LB) medium (10 g/L tryptone, 5 g/L yeast extract, and 10 g/L NaCl) or on LB agar plates. Terrific Broth (TB) medium (5 g/L glycerol, 12 g/L tryptone, 24 g/L yeast extract, 2.3 g/L KH<sub>2</sub>PO<sub>4</sub> and 12.54 g/L K<sub>2</sub>HPO<sub>4</sub>) was used for shake flask fermentation. Antibiotics were used for selections: kanamycin, 50 µg/mL; chloramphenicol, 5 µg/mL; zeocin, 100 µg/mL; spectinomycin, 100 µg/mL; erythromycin, 0.75 µg/mL; rifampicin, 50 µg/mL.

Shake flask fermentation: For β-lactoglobulin (β-Lg) expression, a single colony was inoculated into LB medium and cultured for 12 h to obtain the seed culture. Subsequently, 1 % (v/v) of the seed was transferred into 35 mL of TB medium in a 500-mL shake flask and incubated at 30 °C and 220 rpm. The β-Lg titer was measured after 32 h of fermentation.

Fed-batch fermentation in 5-L fermenter: The fermentation medium consists of 50 g/L yeast extract, 4.2 g/L NaH<sub>2</sub>PO<sub>4</sub>, 11.4 g/L K<sub>2</sub>HPO<sub>4</sub>·3H<sub>2</sub>O, 10 g/L (NH<sub>4</sub>)<sub>2</sub>SO<sub>4</sub>, 5 g/L MgSO<sub>4</sub>·7H<sub>2</sub>O, 0.0675 g/L vitamin B1 and 40 g/L initial glucose. A single colony was inoculated into a 250 mL shake flask containing 10 mL of LB medium and cultured at 37 °C for 10 h to obtain the primary seed culture. Subsequently, 1 % (v/v) of the seed culture was transferred into a 500 mL shake flask containing 25 mL of fermentation medium and incubated under the same conditions until the OD<sub>600</sub> reached 15, yielding the secondary seed culture. The cells were harvested by centrifugation, resuspended in 100 mL of fermentation medium, and inoculated into a 5-L bioreactor containing 1.9 L of fermentation medium. Keep pH at 6.7 using ammonia solution and 8 M HCl and maintain glucose concentration within 10–20 g/L by feeding with 750 g/L glucose throughout the fermentation period. The fermentation temperature was set to 33 °C, with an aeration rate of 1.5 vvm. Dissolved oxygen (DO) was maintained at approximately 35 % by adjusting the agitation speed.

### 2.3. Library construction and screening

All plasmids used in this study are listed in Table 2. The Seamless Cloning Kit was used for library construction. Two adenosine deaminases (TadA8e, TadA9), five cytosine deaminases (CDAN6, hAID\*Δ, hAPOBEC3A, rAPOBEC1, PmCDA1), and 14 fusion protein linkers were employed to construct four libraries: ALib1, ALib2, CLib1, and CLib2 [20]. Base deaminases were selected based on previously reported high-efficiency candidates used in CRISPR-based evolution systems in

**Table 1**  
Strains used in this study.

Names	Characteristics	Source or Reference
<i>E. coli</i> JM110	<i>E. coli</i> JM110	Lab stock
BS168	<i>B. subtilis</i> 168 <i>trpC2</i>	Lab stock
BSXC	BS168 derivative, overexpression of <i>comK</i> gene under the control of xylose-inducible promoter $P_{xytA}$	Lab stock
T7G	BSXC derivative, <i>lctP::P<sub>T7</sub>-gfp</i>	This work
KOT7G	BSXC derivative, <i>lctP::KOP<sub>T7</sub>-gfp</i>	This work
E43	BSXC derivative, <i>amyE::P<sub>Ery</sub>-Ery<sup>R</sup><sub>L43</sub>*(TAA)</i> , with a T7 promoter downstream of <i>Ery<sup>R</sup><sub>L43</sub>*</i>	This work
E43G	E43 derivative, <i>lctP::P<sub>T7</sub>-gfp</i>	This work
E43G-T7RP	E43G derivative harboring plasmid pWL-T7RNAP	This work
KOE43	BSXC derivative, <i>amyE::P<sub>Ery</sub>-Ery<sup>R</sup><sub>L43</sub>*(TAA)</i> , with inactivated T7 promoter downstream of <i>Ery<sup>R</sup><sub>L43</sub>*</i>	This work
E58	BSXC derivative, <i>amyE::P<sub>Ery</sub>-Ery<sup>R</sup><sub>E58G</sub>(GGA)</i> , with a T7 promoter downstream of <i>Ery<sup>R</sup><sub>E58G</sub></i>	This work
E58G	E58 derivative, <i>lctP::P<sub>T7</sub>-gfp</i>	This work
E58G-T7RP	E58G derivative harboring plasmid pWL-T7RNAP	This work
KOE58	BSXC derivative, <i>amyE::P<sub>Ery</sub>-Ery<sup>R</sup><sub>E58G</sub>(GGA)</i> , with inactivated T7 promoter downstream of <i>Ery<sup>R</sup><sub>E58G</sub></i>	This work
BST7RP	BSXC derivative harboring plasmid pWL-T7RNAP	This work
E43-T7RP	E43 derivative harboring plasmid pWL-T7RNAP	This work
EA1-A9	E43 derivative harboring plasmid A1-A9	This work
EA1-C10	E43 derivative harboring plasmid A1-C10	This work
EA1-D6	E43 derivative harboring plasmid A1-D6	This work
EA2-C2	E43 derivative harboring plasmid A2-C2	This work
EA3-A8	E43 derivative harboring plasmid A3-A8	This work
E58-T7RP	E58 derivative harboring plasmid pWL-T7RNAP	This work
EC1-E9	E58 derivative harboring plasmid C1-E9	This work
EC1-G5	E58 derivative harboring plasmid C1-G5	This work
EC2-E5	E58 derivative harboring plasmid C2-E5	This work
EC3-F8	E58 derivative harboring plasmid C3-F8	This work
EC3-G4	E58 derivative harboring plasmid C3-G4	This work
EC5-A2	E58 derivative harboring plasmid C5-A2	This work
EC5-D9	E58 derivative harboring plasmid C5-D9	This work
EC6-C11	E58 derivative harboring plasmid C6-C11	This work
EC6-E6	E58 derivative harboring plasmid C6-E6	This work
EC6-F8	E58 derivative harboring plasmid C6-F8	This work
EC6-H10	E58 derivative harboring plasmid C6-H10	This work
EC8-D12	E58 derivative harboring plasmid C8-D12	This work
E58G-Pugi	E58G derivative harboring plasmid C6-F8-Pugi	This work
E58G-Rugi	E58G derivative harboring plasmid C6-F8-Rugi	This work
E58-T7RP- $P_{ter-ugi}$	E58 derivative harboring plasmid pWL-T7RNAP- $P_{ter-ugi}$	This work
Pugi	E58 derivative harboring plasmid C6-F8-Pugi	This work
Rugi	E58 derivative harboring plasmid C6-F8-Rugi	This work
BS-MutaT7 <sup>A</sup> -X	BSXC derivative, <i>amyE::P<sub>Ery</sub>-Ery<sup>R</sup><sub>L43</sub>*(TAA)</i> , with X bp between the transcription start site of $P_{T7}$ and “TAA”, X = 900, 1200, 1500, 1800, 2100, 3000, 4000, and 5000	This work
BS-MutaT7 <sup>C</sup> -X	BSXC derivative, <i>amyE::P<sub>Ery</sub>-Ery<sup>R</sup><sub>L43</sub>*(TAA)</i> , with X bp between the transcription start site of $P_{T7}$ and “GGA”, X = 855, 1155, 1455, 1755, 2055, 2955, 3955, and 4955	This work
BS-tetK	BSXC derivative, <i>amyE::P<sub>43</sub>-tetK</i> , with the T7 promoter downstream of <i>tetK</i>	This work
A-tetK	BS-TetK derivative harboring plasmid A1-C10	This work
C-tetK	BS-TetK derivative harboring plasmid C6-F8-Pugi	This work
BSF01	BSC01 derivative, $\Delta bpr$ , $\Delta epr$ , $\Delta mpr$ , $\Delta aprE$ , $\Delta nprB$ , $\Delta nprE$ , $\Delta ypr$ , $\Delta wprA$	[37]
BS-P <sub>566</sub> -Lg	BSF01 derivative harboring plasmid pHT01-P <sub>566</sub> - <i>lgb-gfp</i>	This work
BS-codY	BSF01 derivative, <i>amyE::P<sub>43</sub>-codY</i> , with the T7 promoter downstream of <i>codY</i>	This work
A-codY	BS-codY derivative harboring plasmid A1-C10	This work
C-codY	BS-codY derivative harboring plasmid C6-F8-Pugi	This work
A-CodY-Lg-gfp	A-codY derivative harboring plasmid pHT01-P <sub>566</sub> - <i>lgb-gfp</i>	This work
C-CodY-Lg-gfp	C-codY derivative harboring plasmid pHT01-P <sub>566</sub> - <i>lgb-gfp</i>	This work
A10-codY	BS-codY derivative, <i>amyE::codY<sup>(L245P)</sup></i>	This work
C4-codY	BS-codY derivative, <i>amyE::codY<sup>(V171L, D208N)</sup></i>	This work

**Table 1 (continued)**

Names	Characteristics	Source or Reference
A-codY-Lg	A10-codY derivative harboring plasmid pHT01-P <sub>566</sub> - <i>lgb</i>	This work
C-codY-Lg	C4-codY derivative harboring plasmid pHT01-P <sub>566</sub> - <i>lgb</i>	This work

**Table 2**  
Plasmids used in this study.

Names	Characteristics	Source or Reference
pWL	Kan <sup>R</sup> , <i>E. coli</i> - <i>B. subtilis</i> shuttle vector	Lab stock
pHT01	Amp <sup>r</sup> , Cm <sup>r</sup> , <i>E. coli</i> - <i>B. subtilis</i> shuttle vector	Lab stock
pWL-T7RNAP	pWL derivative with T7RNAP cloned under the control of $P_{tet}$ promoter	This work
A1-C10	pWL derivative with $P_{ter}$ -TadA8e-Linker0-T7RNAP cloned	This work
A2-C2	pWL derivative with $P_{ter}$ -TadA8e-Linker1-T7RNAP cloned	This work
C1-E9	pWL derivative with $P_{ter}$ -PmCDA1-Linker0-T7RNAP cloned	This work
C1-G5	pWL derivative with $P_{ter}$ -PmCDA1-Linker0-T7RNAP cloned	This work
C6-E6	pWL derivative with $P_{ter}$ -PmCDA1-Linker2-T7RNAP cloned	This work
C6-F8	pWL derivative with $P_{ter}$ -PmCDA1-Linker5-T7RNAP cloned	This work
pWL-T7RNAP- $P_{ter-ugi}$	pWL-T7RNAP derivative with <i>ugi</i> gene cloned under the control of $P_{tet}$ promoter	This work
C6-F8-Pugi	C6-F8 derivative with <i>ugi</i> gene cloned under the control of $P_{tet}$ promoter	This work
C6-F8-Rugi	C6-F8 derivative with RBS- <i>ugi</i> gene cloned	This work
pHT01-P <sub>566</sub> - <i>lgb-gfp</i>	pHT01 derivative with <i>lgb-gfp</i> gene cloned under the control of $P_{566}$ promoter	This work
pHT01-P <sub>566</sub> - <i>lgb</i>	pHT01 derivative with <i>lgb</i> gene cloned under the control of $P_{566}$ promoter	This work

*B. subtilis*. The sequences of the seven deaminases were listed in Supplementary Sequence S2 and S3. The 14 protein linker candidates used in this study were selected based on their diverse structural characteristics and common applications in fusion protein engineering. These linkers differ in amino acid composition, length, and biophysical properties such as flexible, rigid. The sequences and characteristics of protein linkers are listed in [Supplementary Table S4](#). The temperature-sensitive plasmid pWL- $P_{tet}$  served as the initial plasmid vector and the anhydrotetracycline-inducible promoter  $P_{tet}$  was employed to express the fusion proteins. The plasmid pWL-T7RNAP was used as the backbone for library construction. The sequence of pWL-T7RNAP plasmid was listed in Supplementary Sequence S1.

For ALib1 and CLib1, linkers were added to the C-terminus of each deaminase using primers, ensuring that the sequence at the 3' end of each linker matched the first 25 bp of the N-terminal sequence of T7RNAP (aacacgattaacatcgtaagaacg). Similarly, primers were designed to add the 25 bp sequence (gacaaccccaaggaggtgggatcc) required for insertion into the backbone to the N-terminus of deaminase. Equimolar mixtures of the resulting deaminase-linker fragments were mixed and seamlessly inserted into pWL-T7RNAP, followed by transformation into *E. coli* to obtain sufficient transformants. The colonies were then washed and mixed plasmids were extracted. Finally, the mixed plasmids were separately transformed into *B. subtilis* E43G and E58G to generate ALib1 and CLib1. For ALib2 and CLib2, linkers were added to the N-terminus of the deaminases, with the sequence at the 5' end of each linker matching the 25 bp of the C-terminal sequence of T7RNAP (cttagagtcggactcgcttcgcg). Additionally, primers were used to add the 25 bp DNA sequence (taactgcagtataatcagaacacg) required for insertion into the backbone to the C-terminus of deaminase. The remaining steps were the same as for ALib1 and CLib1, yielding ALib2 and CLib2

libraries.

**Preliminary screening method:** Colonies from ALib1, ALib2, and CLib2 were inoculated into a 96-well plate for pre-culturing about 12 h. Cultures were transferred to LB medium at a 0.5 % inoculation ratio with 0.5  $\mu\text{M}$  anhydrotetracycline (aTC) to induce fusion protein expression, incubating at 30 °C, 750 rpm for 12 h and fluorescence intensity (FI) was measured. Cultures were subsequently diluted 1:1000 into LB medium containing 0.75  $\mu\text{g}/\text{mL}$  erythromycin and incubated for 10 h before measuring cell densities (absorbance at 600 nm,  $\text{OD}_{600}$ ). Finally, transformants were selected for re-screening based on relative fluorescence intensity (RFI) and  $\text{OD}_{600}$ . For CLib1, mixed plasmids were directly transformed into E58G and plated onto LB agar plates containing 0.5  $\mu\text{M}$  aTC, and fluorescence expression was observed.

**Re-screening method:** Selected colonies were inoculated in triplicate into a 96-well plate with LB medium. After pre-culturing for 12 h, cultures were diluted 1:1000 into LB medium containing 0.5  $\mu\text{M}$  aTC and incubated at 30 °C, 750 rpm for 20 h. FI was measured. Cultures were then plated onto both selective (0.75  $\mu\text{g}/\text{mL}$  erythromycin) and non-selective LB agar plates after appropriate dilution. After 20 h incubation, viable cells under each condition were counted and the mutation rates were calculated.

#### 2.4. SDS-PAGE analysis

For intracellular expression of  $\beta\text{-Lg}$ , harvested cells were resuspended in PBS buffer and then lysed using an ultrasonic cell disruptor under ice-bath conditions. After centrifugation, the soluble intracellular fraction and the lysed cell debris were separated. The cell debris was subsequently resuspended in an equal volume of PBS. For SDS-PAGE analysis, protein samples were mixed with  $4 \times$  loading buffer, boiled, and centrifuged. The samples were separated on a 10 % SDS-PAGE gel and electrophoresed using MES SDS running buffer (Thermo Scientific, USA). After electrophoresis, the gel was stained with Coomassie Brilliant Blue R-250 staining solution (Beyotime Biotechnology, Shanghai, China) for visualization. The titer of bovine  $\beta\text{-Lg}$  was quantified by the Bradford method (Beyotime Biotech, Shanghai, China).

#### 2.5. Assay of fluorescence intensity

The GFP fluorescence intensity (excitation wavelength-488nm; emission wavelength-523nm) and  $\text{OD}_{600}$  were measured using a microplate Multi-Mode Reader (BIOTEK, Cytation 3). The background  $\text{OD}_{600}$  from LB medium and fluorescence intensity from strain without GFP expression were subtracted. The RFI was represented with normalization at  $\text{OD}_{600}$ .

#### 2.6. Flow cytometry analysis

Flow cytometry was performed using a BD FACSAria III equipped with BD FACSDiva software (BD Biosciences). Briefly, 0.5 mL of cultured cells was harvested and washed three times with PBS, then resuspended in filtered PBS to an  $\text{OD}_{600}$  of 0.5. Samples were analyzed with excitation at 488 nm and emission was detected using a 523/21 nm bandpass filter. For each sample, at least 10,000 events were collected. Forward scatter (FSC) and side scatter (SSC) signals were logarithmically amplified, and appropriate gating was applied to exclude background noise. Data were analyzed and visualized using FlowJo software.

#### 2.7. Mutation rate calculation

Luria–Delbrück fluctuation analysis was performed to determine the mutation rate of BS-MutaT7 [38]. The target pWT-deaminase-linker-T7RNAP plasmids were reconstructed and transformed into E43 and E58. Three single colonies were picked, inoculated into a 96-well plate and cultured for 12 h. Cultures were then diluted 1:1000 into LB medium containing the inducer and incubated at

30 °C, 750 rpm for 20 h until saturation. The cultures were subsequently plated onto selective and non-selective LB agar plates and viable cells under each condition were counted to calculate the target and untargeted mutation rates. Mutation rates were estimated using FluCalc and analyzed using the Maximum Synonymous Substitution (MSS) maximum likelihood method. Mutation rates per generation per base  $\mu$  (s.p.b.) were further calculated using the formula:  $\mu$  (s.p.b.) =  $m/(R \times G)$ , where  $m$  is the mutation rate estimated by FluCalc [39];  $R$  is the number of distinct mutational events that make the resistance gene effective and  $R = 1$  in this study;  $G$  represents the generations number of mutations accumulated and one passage counts as 10 generations.

#### 2.8. Continuous evolution of tigeicycline resistance

For the evolution of *tetK*, encoding the tetracycline efflux transporter TetK, which confers tigeicycline resistance in cells. The experiments were conducted in LB medium supplemented with 50  $\mu\text{g}/\text{mL}$  kanamycin and 0.5  $\mu\text{M}$  aTC at 30 °C. The initial tigeicycline concentration was set at 0.25  $\mu\text{g}/\text{mL}$ . Once noticeable growth was observed at the given tigeicycline concentration, a 2 % inoculum was transferred into LB medium with a higher tigeicycline concentration to continue the evolutionary process. After evolution, the resulting mutants were streaked onto plates for isolation and seven single colonies were analyzed by sanger sequencing. The sequence of *tetK* gene was listed in Supplementary Sequence S4.

#### 2.9. Continuous evolution of the global transcriptional regulator CodY

For the evolution of global transcriptional regulator *CodY*, experiments were carried out in LB medium at 30 °C. Transformants co-harboring the *P<sub>43-codY</sub>* expression cassette, the mutagenesis plasmid and the pHT01-*P<sub>566-lgb-gfp</sub>* plasmid were cultured in LB medium. The T7 promoter was placed downstream of the *codY* gene in reverse orientation to its coding sequence. Seed cultures were inoculated at a 1 % (v/v) into LB medium supplemented with 50  $\mu\text{g}/\text{mL}$  kanamycin, 5  $\mu\text{g}/\text{mL}$  chloramphenicol, and 0.5  $\mu\text{M}$  aTC for evolution. After 20 h of induction, cultures were passaged with a 1 % (v/v) inoculum into the same medium for the next round of mutagenesis. Following two rounds of mutagenesis, clones with high fluorescence were isolated by flow cytometry. The sorted population underwent an additional two rounds of mutagenesis and flow cytometric screening. High-fluorescence cells obtained from the final round were plated on LB agar plates containing 5  $\mu\text{g}/\text{mL}$  chloramphenicol. Ten single colonies from each system were selected for re-screening, and the transformants with the highest fluorescence intensity were chosen for sequencing analysis.

### 3. Results and discussions

#### 3.1. Design of the BS-MutaT7 system for genome mutagenesis in *B. subtilis*

The schematic illustration of the T7 RNA polymerase-guided base editor system in this study is shown in Fig. 1a. To test its mutagenic activity, two inactive erythromycin resistance genes (*Ery<sup>R</sup>*) were designed as model target genes (Fig. 1b). The sequence of active erythromycin resistance gene *Ery<sup>R</sup>* was listed in Supplementary Sequence S5. The promoter *P<sub>Ery</sub>* was used to express erythromycin resistance gene, while the T7 promoter was placed downstream of *Ery<sup>R</sup>*, in reverse orientation to its coding sequence. To enable plasmid loss after mutagenesis, temperature-sensitive plasmids were constructed to express the fusion proteins.

To specifically test the mutagenic activity of BS-MutaT7<sup>A</sup>, a stop codon reversion assay was performed by introducing “TAA” at the position 43 (L43\*) of the *Ery<sup>R</sup>* gene. When adenosine deaminase induces an A:T > G:C transition in template strand, mutating “TAA” to the sense codon “CAA”, cell regain erythromycin resistant. For BS-MutaT7<sup>C</sup>, an

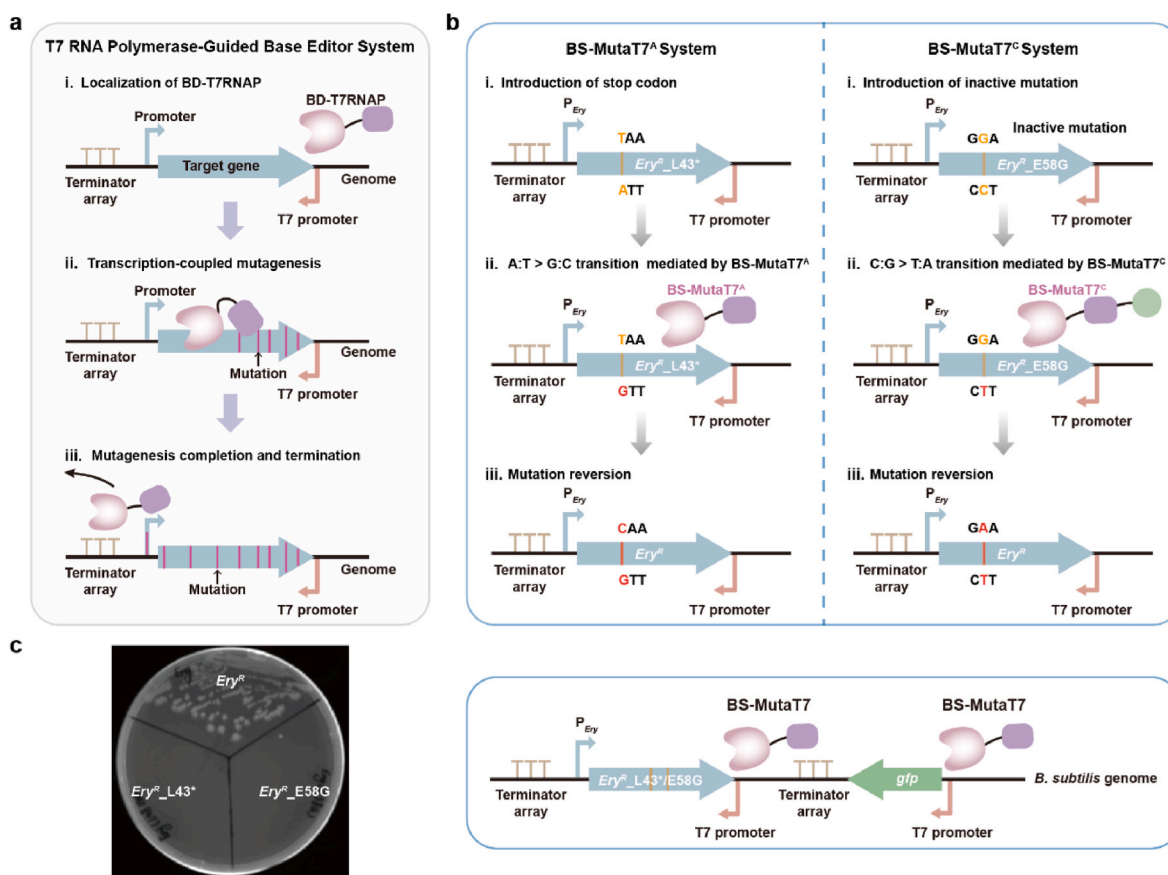


**Fig. 1.** Graphic summary of the BS-MutaT7 system in *B. subtilis*. (a) Schematic of the T7 RNA polymerase-guided base editor system. Temperature-sensitive plasmids were constructed to express the fusion protein comprising the base deaminase and T7RNAP. The fusion protein specifically binds to the T7 promoter inserted downstream of the target gene on the genome. As the T7 RNAP transcribes along the target gene, the deaminase introduces point mutations. Upon encountering the T7 terminator array, the fusion protein detaches from the DNA, terminating transcription and mutagenesis. The mutagenesis plasmid is lost by increasing the cultivation temperature. BD-T7RNAP: chimeric fusion of base deaminase with T7RNAP. (b) Representation of the reporter *Ery<sup>R</sup>* expression cassettes and transcriptional activities of the BS-MutaT7 system. In BS-MutaT7<sup>A</sup>, the distance from the T7 transcription start site (TSS) to the “TAA” codon was 616 bp, while in BS-MutaT7<sup>C</sup>, the distance to “GGA” codon was 571 bp. The green circle represented the *ugi* gene. The bold bases represented the target sites for mutagenesis. The RFI was used to assess the transcriptional activity. (c) Verification of *Ery<sup>R</sup>* gene mutation inactivation. The *B. subtilis* strains carrying *Ery<sup>R</sup>\_L43\** (“TAA” stop codon) or *Ery<sup>R</sup>\_E58G* (inactive mutation) cassettes were erythromycin sensitive and unable to grow on selective LB agar plates containing 0.75 µg/mL erythromycin.

inactive mutation was introduced at position 58 (E58G) in *Ery<sup>R</sup>* gene by replacing “GAA” with “GGA” triplets (Fig. 1c). Only when cytosine deaminase induces an C:G > T:A transition in template strand, mutating “GGA” back to the original codon “GAA”, erythromycin resistance can be restored. To terminate mutagenesis, the T7 terminator array was added downstream of the target gene. We integrated the two inactive expression cassettes into the *B. subtilis* genome to generate E43 and E58. Restoration of erythromycin resistance in cells represents the mutagenic activity of the BS-MutaT7 system. Additionally, to assess both mutagenic and transcriptional activity, the *P<sub>T7</sub>-gfp* expression cassette was integrated into the genome of E43 and E58, generating E43G and E58G (Fig. 1b). The expression of *gfp* was under the control of *P<sub>T7</sub>* and the RFI was used to evaluate the transcriptional activity of BS-MutaT7 system.

### 3.2. Construction and screening of the adenosine deaminase-T7RNAP mutagenesis library

To develop a high activity BS-MutaT7<sup>A</sup>, TadA8e, TadA9 and 14 fusion protein linkers were selected to construct two libraries (ALib1 and ALib2), with E43G as the initial strain (Fig. 2a). The primary difference between ALib1 and ALib2 is the position of deaminase, which is fused either to the N-terminus or C-terminus of T7RNAP. A total of 280 single colonies were randomly selected from each library for preliminary

screening. Following inducing the expression of the fusion proteins, FL was measured. Cultures were then transferred to selective medium and incubated for 12 h for measuring OD<sub>600</sub>. Only colonies with high mutagenic and transcriptional activity were able to grow on the selective medium and exhibited detectable fluorescence. The results revealed that almost all colonies from ALib2 showed no fluorescence and failed to grow on the selective medium, while most colonies from ALib1 displayed detectable fluorescence (Supplementary Tables S1 and S2). This indicated that ALib2 lost both transcriptional and mutagenic activity. Since the C-terminal of T7RNAP is the polymerization domain, we hypothesize that the fusion of deaminase to the C-terminus of T7RNAP may affect its polymerization activity in *B. subtilis*. Subsequently, 30 single clones from ALib1 were selected for re-screening, with three replicates per clone, and both FI and target mutation rates were measured. Re-screening results demonstrated that most adenosine deaminase-T7RNAP fusion proteins retained some T7RNAP transcriptional activity, although the fusion negatively impacted its activity. Among the tested clones, A1-A9, A1-C10, A1-D6, A2-C2, and A3-A8 showed relatively high mutation rates (Fig. 2b). Notably, A2-B8 exhibited the highest mutation rate but lacked the transcriptional activity.

To more accurately assess the target mutation rates of A1-A9, A1-C10, A1-D6, A2-C2 and A3-A8, fusion protein plasmids were individually transformed into E43, which contains only the *Ery<sup>R</sup>\_L43\** without

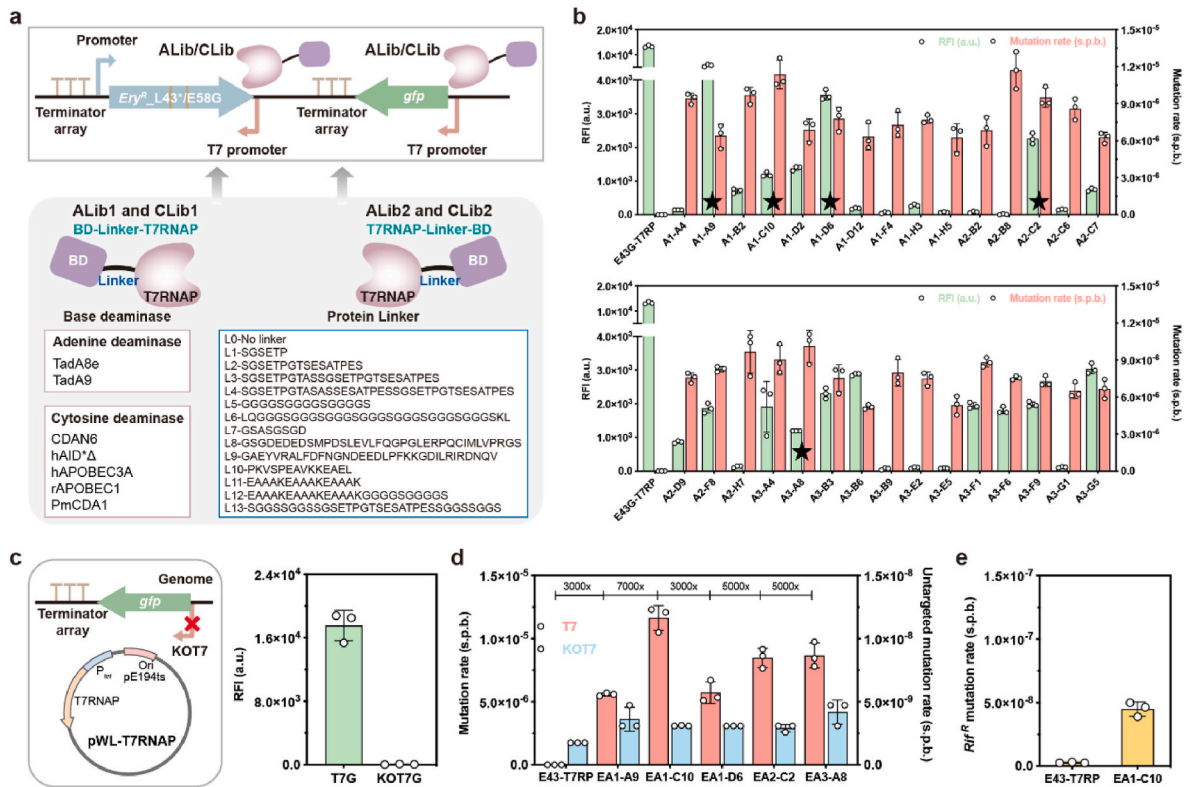


**Fig. 2.** Construction and screening of BS-MutaT7<sup>A</sup> with transcriptional and mutagenic activity in *B. subtilis*. (a) Schematic of the BD-T7RNAP mutagenesis library construction. The plasmid vector pWL-P<sub>tet</sub> was used to express BD-T7RNAP fusion proteins, induced by 0.5 μM aTc. (b) Transcriptional and mutagenic activity analysis of 30 single colonies from ALib1 during preliminary screening. The host strain E43G contained two cassettes: the reporter *Ery<sup>R</sup>\_L43<sup>\*</sup>/E58G* expression cassette and the *P<sub>T7</sub>-gfp* expression cassette. An asterisk indicated strains with relatively high mutation rates selected for rescreeing. (c) Validation of the inactivated promoter KOT7. The FI assay was used to assess the KOT7 activity and the KOT7G strain exhibited no measurable fluorescence. (d) Analysis of the target mutation rate and untargeted mutation rate of the screened strains. Plasmids were transformed into E43 to evaluate the mutation rates, identifying EA1-C10 as the optimal BS-MutaT7<sup>A</sup> with the highest target mutation efficiency. The *P<sub>T7</sub>* promoters in the C-terminus of *Ery<sup>R</sup>\_L43<sup>\*</sup>* expression cassette of the strains were replaced with KOT7 to assess the untargeted mutation rates. The numbers indicated the fold increase in target mutation rates compared to the genomic spontaneous mutation rate. (e) Evaluation of the genomic off-target mutations in BS-MutaT7<sup>A</sup>. The rifampicin resistance assay was used to test the off-target mutation rate. Induced cultures were plated on LB agar plates containing 50 μg/mL rifampicin for colony counting and fluctuation analysis. Error bar represents data from biological triplicate.

the *P<sub>T7</sub>-gfp* expression cassette. Compared to the control strain E43-T7RP carrying the pWL-T7RNAP plasmid, the five fusions exhibited significant mutagenic activities. Fluctuation analysis revealed that EA1-C10 had the highest mutation efficiency, reaching  $1.2 \times 10^{-5}$  per generation per base (s.p.b.), which was 7000-fold higher than the host genomic mutation rate ( $1.5 \times 10^{-9}$  s.p.b.). For other fusions, the target mutation rates were  $5.7 \times 10^{-6}$  s.p.b. for EA1-A9 and EA1-D6,  $8.5 \times 10^{-6}$  s.p.b. for EA2-C2, and  $8.7 \times 10^{-6}$  s.p.b. for EA3-A8. To assess untargeted mutation rates and confirm overall targeting efficiency, the *P<sub>T7</sub>* in the C-terminus of *Ery<sup>R</sup>\_L43<sup>\*</sup>* expression cassette was replaced with KOT7, an inactive variant of *P<sub>T7</sub>*. The *P<sub>T7</sub>* promoter was inactivated by an insertion to create KOT7 (Supplementary Fig. S1). GFP was expressed under the control of KOT7 on the genome and RFI analysis confirmed that KOT7 was non-functional (Fig. 2c). Fluctuation analysis showed that the untargeted mutation rate for EA1-C10 was  $3.1 \times 10^{-9}$  s.p.b., while EA2-C2 exhibited the lowest untargeted mutation rate at  $2.9 \times 10^{-9}$  s.p.b., both values comparable to the control E43-T7RP. host genomic mutation rate (Fig. 2d). Remarkably, the target mutation rate of EA1-C10 was 3800-fold higher than that of the KOT7. To assess leakage, we tested the target mutation rate of EA1-C10 without inducer was  $2.8 \times 10^{-7}$  s.p.b. and the ratio between induced (+aTc) and non-induced (−aTc) conditions was 41:1 (Supplementary Fig. S2). This confirmed that the observed mutations were dependent on the presence of *P<sub>T7</sub>* and not caused by off-target events. Among all candidates, EA1-C10 was identified as the optimal BS-MutaT7<sup>A</sup> through library screening in *B. subtilis*. Sequencing analysis revealed that EA1-C10 was a chimeric mutator,

where TadA8e was directly fused to the N-terminus of T7RNAP without a linker (L0), whereas in EA2-C2, TadA8e and T7RNAP were fused via linker1 (L1).

During *in vivo* mutagenesis, genomic off-target mutations can impair cell growth if essential genes are mutated. In *B. subtilis*, rifampicin resistance (*Rif<sup>R</sup>*) arises from mutations in the *rpoB* gene, which encodes the β-subunit of RNA polymerase [40]. Thus, the rifampicin resistance assay employed to assess the off-target mutation rate of BS-MutaT7<sup>A</sup>. Fluctuation analysis showed that the rifampicin resistance mutation rate of EA1-C10 was  $4.5 \times 10^{-8}$  s.p.b., approximately 16-fold higher than the control strain, likely due to the high activity of TadA8e (Fig. 2e). Nevertheless, the off-target mutation rate was three orders of magnitude lower than the target mutation rate, indicating that while BS-MutaT7<sup>A</sup> caused some off-target mutations, their impact was minimal.

### 3.3. Construction and screening of the cytosine deaminase-T7RNAP mutagenesis library

To construct and screen high-activity BS-MutaT7<sup>C</sup>, five cytosine deaminases (CDAN6, hAID\*Δ, hAPOBEC3A, rAPOBEC1, PmCDA1) with consistent fusion protein linkers were used to create two libraries, CLib1 and CLib2 (Fig. 2a). The main difference between CLib1 and CLib2 was the position of cytosine deaminase, either at the N-terminus (CLib1) or C-terminus (CLib2) of T7RNAP. From CLib1, 844 single colonies were randomly selected for preliminary screening. Based on the results from ALib2, the screening method for CLib2 was adjusted. After

transformation of the library plasmids into E58G, the cultures were plated on LB inducer plates and incubated for 20 h, followed by direct visual inspection of colony fluorescence. CLib2 colonies exhibited no green fluorescence, indicating a lack of transcriptional activity, and were excluded from further analysis. In contrast, numerous CLib1 colonies displayed fluorescence, confirming transcriptional activity (Supplementary Fig. S3). The FI and OD<sub>600</sub> in the selective medium of CLib1 were measured (Supplementary Table S3). From CLib1, 40 colonies were selected for detailed screening with three replicates per clone. All cytosine deaminase-T7RNAP fusions retained transcriptional activity and 12 strains exhibited relatively high mutation rates (Fig. 3a). To assess the target and untargeted mutation rates, the 12 plasmids of fusion proteins were transformed into E58 and KOE58 (lacking the P<sub>T7</sub>-gfp expression cassette). Among them, EC6-F8 achieved the highest mutation rate of  $1.6 \times 10^{-6}$  s.p.b., approximately 1000-fold higher than the host genomic mutation rate (Fig. 3b). Other chimeric mutants, including EC6-E6 ( $8.4 \times 10^{-7}$  s.p.b.), EC1-E9 ( $7.3 \times 10^{-7}$  s.p.b.), and EC1-G5 ( $7.0 \times 10^{-7}$  s.p.b.), also demonstrated significant mutation rates. Fluctuation analysis revealed that the untargeted mutation rate of EC6-F8 was  $7.4 \times 10^{-9}$  s.p.b., five-fold higher than the control E58-T7RP (Fig. 3b). Leakage testing of EC6-F8 showed that the target mutation rate without inducer was  $1.6 \times 10^{-7}$  s.p.b. and the ratio between induced (+aTc) and non-induced (−aTc) conditions was 10:1 (Supplementary Fig. S4). Sequencing revealed that all high-activity plasmids carried the same cytosine deaminase, PmCDA1. In EC6-F8, PmCDA1 was fused to the N-terminus of T7RNAP using a (GGGGS)<sub>3</sub> linker, designated as L5. whereas EC6-E6 employed linker 2 (L2). In EC1-E9 and EC1-G5, PmCDA1 were fused without linker (L0).

To enhance the mutation rate of EC6-F8, UGI, an inhibitor of uracil-DNA glycosylase (UNG), was introduced to prevent the removal of uracil residues. Two strategies were employed to co-express the *ugi* gene in C6-

F8 plasmid (Fig. 3c). The first strategy involved placing the *ugi* gene under the control of P<sub>tet</sub> promoter to construct plasmid C6-F8-Pugi and the second strategy involved fusing the RBS-*ugi* sequence to the C-terminal of T7RNAP to construct plasmid C6-F8-Rugi. To test whether the expression of *ugi* affected the transcriptional activity of T7RNAP, two constructs were transformed into E58G to measure the RFI and found that it had minimal impact on transcriptional activity (Supplementary Fig. S5). Both constructs were then transformed into E58 to test the genome editing efficiency. As shown in Fig. 3c, both significantly increased the target mutation rate. Pugi achieved a target mutation rate of  $5.8 \times 10^{-5}$  s.p.b., a 36-fold increase over EC6-F8 and 37,000-fold higher than the genomic mutation rate, with a slightly elevated untargeted mutation rate of  $1.7 \times 10^{-8}$  s.p.b. compared to EC6-F8. The target: untargeted mutation ratio for Pugi was 3400:1 and its target mutation rate under induction (+aTc) was 126 times higher than without induction (−aTc) (Fig. 3c and Supplementary Fig. S4). Rugi reached a target mutation rate of  $4.3 \times 10^{-5}$  s.p.b., a 28,000-fold increase over the genomic mutation rate, but exhibited a higher untargeted mutation rate than Pugi. Through library screening and optimization, Pugi was identified as the optimal BS-MutaT7<sup>C</sup> in *B. subtilis*.

The rifampicin resistance assay was employed to evaluate the off-target mutation rate of BS-MutaT7<sup>C</sup>. The E58 harboring the plasmid pWL-T7RNAP-P<sub>tet</sub>-*ugi*, where *ugi* was expressed under the control of P<sub>tet</sub> promoter, showed no significant increase in the off-target mutation rate compared to the strain expressing only T7RNAP (Fig. 3d). With BS-MutaT7<sup>C</sup> expression, the off-target mutation rate increased slightly to  $2.3 \times 10^{-8}$  s.p.b. compared to the negative control. In conclusion, the BS-MutaT7<sup>C</sup> system achieved the high on-target mutation rates while maintaining minimal off-target mutagenesis.

The expression level of the fusion protein directly influences mutation efficiency. To optimize target mutagenesis, aTc was tested at

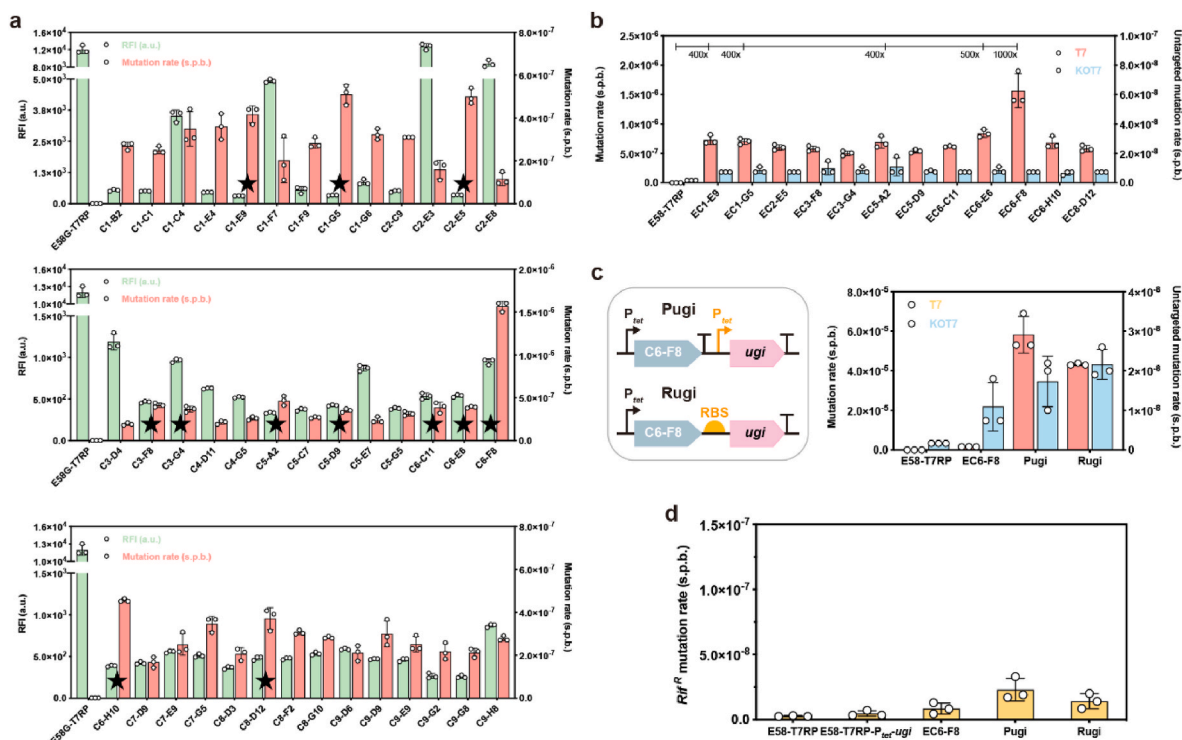


**Fig. 3.** Construction and optimization of BS-MutaT7<sup>C</sup> with transcriptional and mutagenic activity in *B. subtilis*. (a) Transcriptional and mutagenic activity of 40 single colonies from CLib1 during preliminary screening. The host strain E58G contained two cassettes: the reporter *Ery<sup>R</sup>*\_E58G expression cassette and P<sub>T7</sub>-gfp expression cassette. An asterisk indicated plasmids with relatively high mutation rates selected for rescreening. (b) Analysis of the target mutation rate and untargeted mutation rate of the screened strains. Plasmids were transformed into E58 to evaluate the mutation rates, with EC6-F8 achieving the highest target mutation efficiency. The numbers indicated the fold increase in target mutation rates compared to the genomic spontaneous mutation rate. (c) Engineering the *ugi* expression to enhance the target mutation efficiency. (d) Evaluation of the genomic off-target mutations in BS-MutaT7<sup>C</sup>. The plasmid pWL-T7RNAP-P<sub>tet</sub>-*ugi* was transformed into E58 to evaluate the effect of *ugi* expression on off-target mutation rate. Error bar represents data from biological triplicate.

induction concentrations of 0.25  $\mu\text{M}$ , 0.5  $\mu\text{M}$ , and 0.75  $\mu\text{M}$ . The initially applied 0.5  $\mu\text{M}$  concentration yielded the highest mutation rates (Supplementary Fig. S6). At a concentration of 0.25  $\mu\text{M}$ , the mutation rates of both systems significantly decreased, with reductions of 32.14 % in the BS-MutaT7<sup>A</sup> system and 51.42 % in the BS-MutaT7<sup>C</sup> system, likely due to insufficient induction of both the fusion protein and UGI. Higher induction at 0.75  $\mu\text{M}$  also led to reduced mutation rates by 20.80 % and 25.95 % in the BS-MutaT7<sup>A</sup> and BS-MutaT7<sup>C</sup> systems, respectively. These results indicated that 0.5  $\mu\text{M}$  aTC achieved optimal induction for efficient fusion protein expression and maximal target mutagenesis.

### 3.4. Testing the sustained mutagenic activity of BS-MutaT7

To enable continuous evolution of long genes and operons on the genome, the sustained mutagenic activity of BS-MutaT7 is critical. To test this, the distance between the mutated base and the P<sub>T7</sub> transcription start site were adjusted to 900 bp, 1200 bp, 1500 bp, 1800 bp, 2100 bp, 3000 bp, 4000 bp and 5000 bp by repositioning P<sub>T7</sub> in BS-MutaT7<sup>A</sup> (Fig. 4a). Similarly, for BS-MutaT7<sup>C</sup>, the distances were set to 855 bp, 1155 bp, 1455 bp, 1755 bp, 2055 bp, 2955 bp, 3955 bp, and 4955 bp (Fig. 4a). The results showed that BS-MutaT7 maintained relatively high mutagenic activity even with an extended editing window of 5000 bp (Fig. 4b and c). As shown in Fig. 4b, the mutation rate of BS-MutaT7<sup>A</sup> at 5000 bp was  $5.8 \times 10^{-6}$  s.p.b., representing a 55.3 % reduction compared to its initial rate at 616 bp. Notably, the mutation rate remained stable when the editing window was within 2 kb. Similarly, for BS-MutaT7<sup>C</sup>, mutagenic activity gradually decreased with increasing editing window, reaching  $2.9 \times 10^{-5}$  s.p.b. at 4955 bp, which represented a 49.0 % reduction compared to its initial rate at 571 bp (Fig. 4c). Despite this decrease, the mutation rate was still 18,000-fold higher than the genomic mutation rate. These findings confirmed the effectiveness and stability of BS-MutaT7 system for *in situ* evolution of longer genomic target regions.

Compared with existing *in vivo* continuous evolution platforms, BS-MutaT7 enables target, high-frequency mutagenesis in *B. subtilis* with the guidance of T7RNAP. This system exhibits strong target specificity, high processivity, and the low off-target mutation rate, allowing for stable and efficient editing of large genomic regions. Furthermore, BS-MutaT7 operates independently of viral replication machinery, thereby offering a simple and effective alternative for genome-scale continuous evolution. Importantly, it also addresses the key limitations of CRISPR-based systems, such as narrow editing windows and the requirement for multiple gRNAs.

### 3.5. Accelerated continuous evolution of tigecycline resistance

As a proof of concept, the BS-MutaT7 system was applied to evolve the gene *tetK*, encoding the tetracycline efflux transporter, which confers tigecycline resistance in cells. The *tetK* gene was under the control of constitutive promoter P<sub>43</sub>, while the T7 promoter was placed the downstream of *tetK* gene in the reverse orientation to its coding

sequence (Fig. 5a). The expression cassette was integrated into the genome, generating BS-tetK. Two plasmids, A1-C10 and C6-F8-Pugi, were transformed into BS-tetK to create A-tetK and C-tetK for continuous hypermutation. Three independent transformants were cultured separately and passaged continuously in centrifuge tubes with increasing tigecycline concentration (Fig. 5a). If two transformants failed to grow at a specific tigecycline concentration, the surviving one was inoculated three replicates for the next round. The tigecycline concentration of 0.25  $\mu\text{g/mL}$  served as the initial concentration. For comparison, cells containing the P<sub>43</sub>-*tetK* expression cassette without mutagenesis plasmid were able to grow on agar plates with 0.25  $\mu\text{g/mL}$  tigecycline but not at 0.5  $\mu\text{g/mL}$  (Fig. 5b). By progressively increasing tigecycline concentrations during multiple rounds of *in vivo* hypermutation, the evolved *tetK* gene conferred tigecycline resistance up to 8  $\mu\text{g/mL}$  within 10 days, representing a 16-fold increase in BS-MutaT7<sup>A</sup> (Fig. 5b). Similarly, it conferred resistance up to 6  $\mu\text{g/mL}$ , representing a 12-fold increase in BS-MutaT7<sup>C</sup> (Fig. 5c).

The synonymous and nonsynonymous mutations were identified on the *tetK* gene in BS-MutaT7 system. In BS-MutaT7<sup>A</sup>, V128A, F233L, Y282H, W350R, and Y425H mutations were enriched, alongside numerous mutations in the P<sub>43</sub> promoter were identified (Fig. 5b and d). The editable window spanned 1737 bp, with the most distal mutation located in the P<sub>43</sub> promoter region, 1526 bp downstream of the T7 transcription start site. Meanwhile, a small number of A to G transitions were detected on the coding strand of *tetK* gene, corresponding to the template strand for the AD-T7RNAP fusion. However, A to G transitions on the non-template strand of the AD-T7RNAP fusion remained predominant. In BS-MutaT7<sup>C</sup>, sanger sequencing identified the enriched mutations D75N, A120T, D201N, D319N, and C214Y (Fig. 5c and d). The most distal mutation introduced was located in the P<sub>43</sub> promoter region, 1685 bp downstream of the T7 transcription start site. In conclusion, *tetK* variants with increased resistance to tigecycline were obtained using the BS-MutaT7 system.

### 3.6. Accelerated continuous evolution of the global transcriptional regulator CodY

$\beta$ -lactoglobulin, the most abundant whey protein in bovine milk, has been successfully synthesized in microbial cell factory such as *E. coli* [41, 42], *S. cerevisiae* [43] and *Pichia pastoris* [44]. Owing to its safety and suitability for protein expression, *B. subtilis* has been engineered for the efficient production of various proteins, including  $\alpha$ -casein [45],  $\alpha$ -lactalbumin [46,37], and human interleukin-3 [47]. Therefore, *B. subtilis* represents a promising host for the heterologous production of bovine  $\beta$ -Lg. The codon-optimized  $\beta$ -Lg sequence is provided in Supplementary Sequence S6. Using the pHT01 vector as the backbone, the constitutive promoter P<sub>566</sub> was employed to express  $\beta$ -Lg. SDS-PAGE analysis of the intracellular insoluble fraction revealed a distinct band with a molecular mass of about 18.4 kDa, consistent with the deduced molecular weight of  $\beta$ -Lg (Fig. 6a). This band was detected in the total intracellular protein but was absent from the soluble fraction, indicating

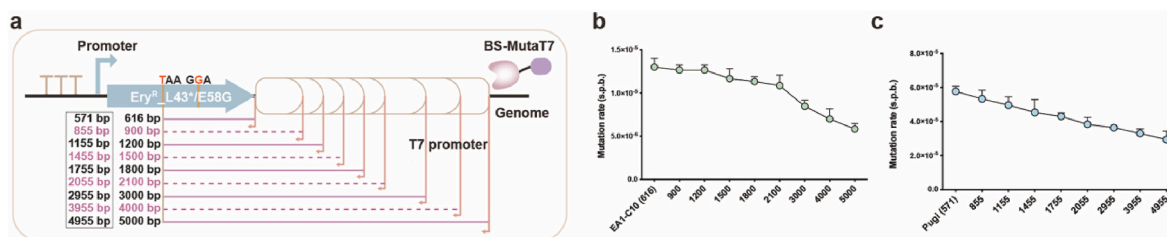


**Fig. 4.** Testing the sustained mutagenic activity of BS-MutaT7<sup>A</sup> and BS-MutaT7<sup>C</sup> in *B. subtilis*. (a) Schematic of the expanded editing window. By repositioning the T7 promoter on the genomes of E43 and E58, the editing window was extended to 5000 bp for BS-MutaT7<sup>A</sup> and 4955 bp for BS-MutaT7<sup>C</sup>. The values in the box represented the corresponding editing window lengths for BS-MutaT7<sup>C</sup>. (b) The sustained mutagenic activity of BS-MutaT7<sup>A</sup>. (c) The sustained mutagenic activity of BS-MutaT7<sup>C</sup>. Error bar represents data from biological triplicate.

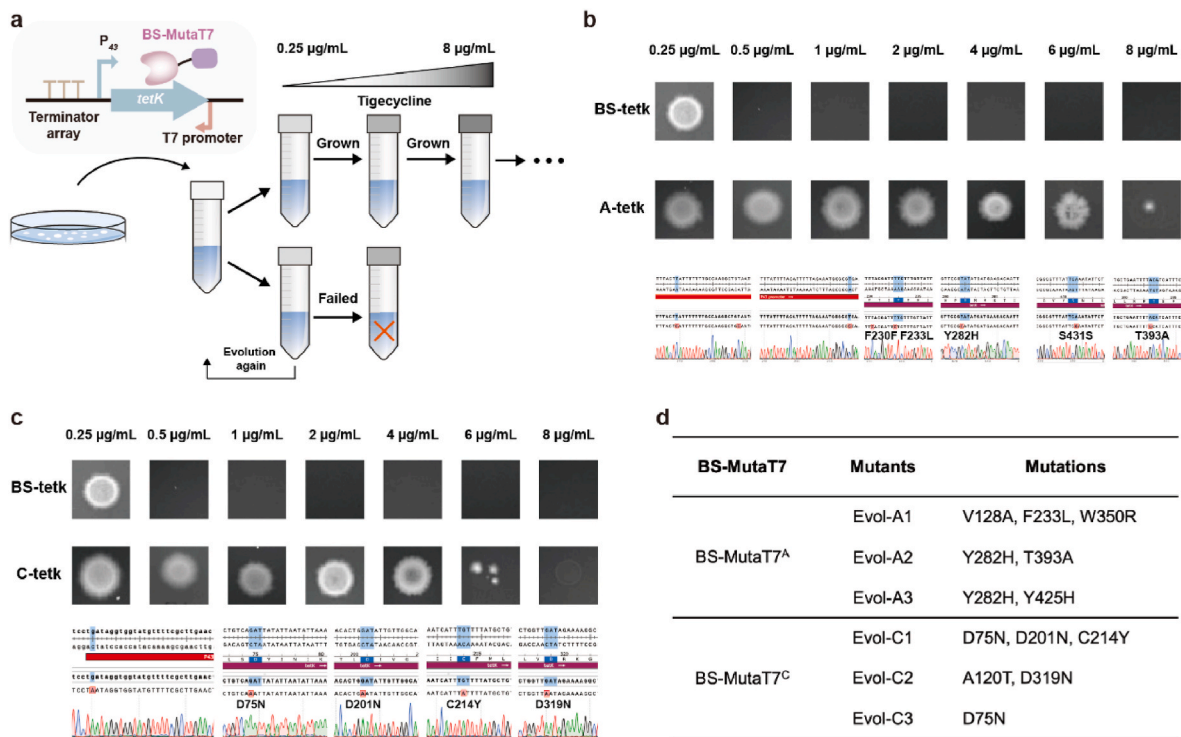


**Fig. 5.** Continuous evolution of tigecycline resistance using the BS-MutaT7 system. (a) Schematic of the continuous evolution process for the *tetK* gene. Using the BS-MutaT7<sup>A</sup> and BS-MutaT7<sup>C</sup> systems, three transformants were cultured separately in centrifuge tubes. (b) Validation of the evolved *tetK* gene using the BS-MutaT7<sup>A</sup> system. Sanger sequencing of the key mutations introduced by BS-MutaT7<sup>A</sup> revealed T to C transitions on the coding strand of *tetK* gene and the P<sub>43</sub> promoter. Several mutants also exhibited additional A to G transitions. The evolved *tetK* gene conferred a 16-fold increase in tigecycline resistance. (c) Validation of the evolved *tetK* gene using the BS-MutaT7<sup>C</sup> system. Sanger sequencing analysis of the key mutations introduced by BS-MutaT7<sup>C</sup> identified G to A transitions on the coding strand of *tetK* gene and the P<sub>43</sub> promoter. The evolved *tetK* gene conferred a 12-fold increase in tigecycline resistance. (d) Most enriched *tetK* mutants identified through continuous evolution with BS-MutaT7 system.

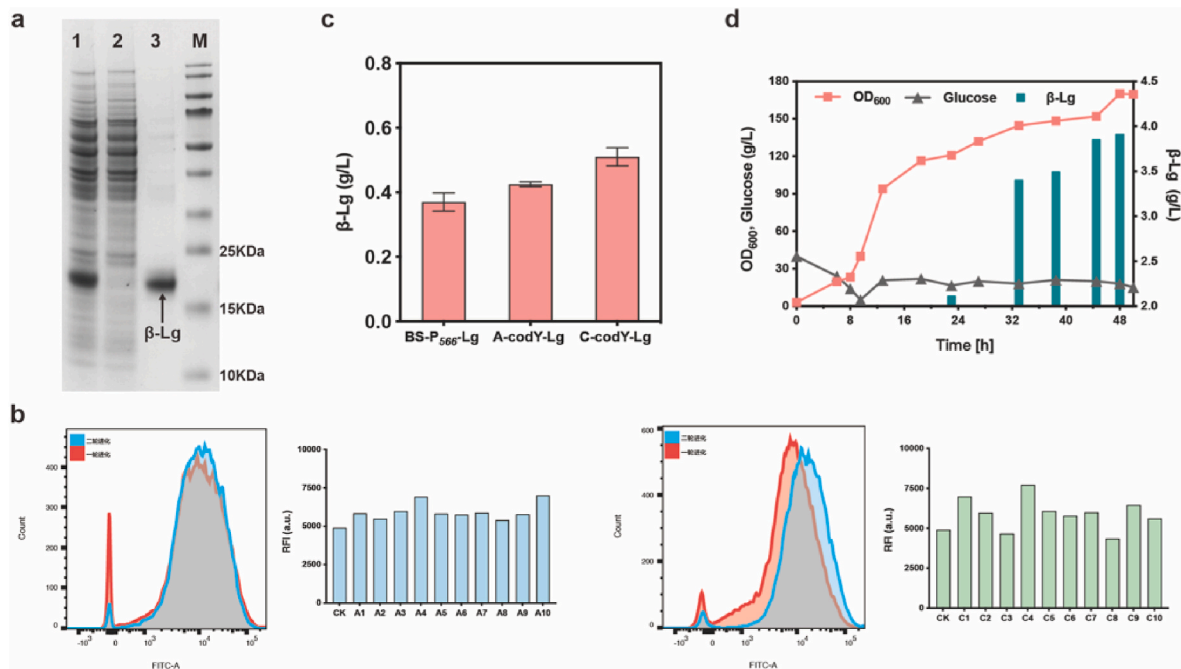


**Fig. 6.** Continuous evolution of global transcriptional regulator CodY using the BS-MutaT7 system. (a) Expression of  $\beta$ -Lg in the *B. subtilis* chassis cells visualized by SDS-PAGE analysis. Lane 1, the total intracellular protein of BS-P<sub>566</sub>-Lg. Lane 2, the intracellular soluble supernatant fraction. Lane 3, the intracellular insoluble fraction. Lane M represents the molecular weights of pre-stained protein marker. (b) Flow cytometric analysis and rescreening of high fluorescence intensity mutants. The left panel represents the screening results in BS-MutaT7<sup>A</sup> system, while the right panel represents the screening results in BS-MutaT7<sup>C</sup> system. (c)  $\beta$ -Lg titers of *codY* mutants, in shake flask fermentation. (d) Fermentation of C-codY-Lg in a 5-L fermenter.

that  $\beta$ -Lg was predominantly expressed in an insoluble form. The titer of  $\beta$ -Lg was 0.37 g/L in shake flask fermentation.

Compared with modifying protein expression elements, engineering global transcriptional regulators enables dynamic reprogramming of gene networks to improve cellular metabolism and boost target protein synthesis [48–50]. To further boost the intracellular expression of  $\beta$ -Lg, the BS-MutaT7 system was employed to evolve the global transcriptional regulator CodY. Cao et al. constructed a *codY* random mutagenesis library in *B. subtilis* and identified a mutant exhibiting a 52 % increase in  $\beta$ -galactosidase activity, which was subsequently used to enhance GFP expression [50,51]. In this study, *codY* was placed under the control of constitutive  $P_{43}$  promoter, with a reverse-oriented T7 promoter inserted downstream of its coding sequence. This expression cassette was integrated into the genome of BSF01 to obtain BS-codY. Subsequently, two mutagenesis plasmids, A1-C10 and C6-F8-Pugi, were introduced into BS-codY to obtain the evolved strains A-codY and C-codY, respectively. Previous studies have shown that fluorescence remained detectable even when the target protein-GFP fusion was expressed in the insoluble fraction [52,53]. To facilitate high-throughput screening, *gfp* was fused to the 3' end of *lgb* to construct the plasmid pHT01- $P_{566}$ -lgb-*gfp*. This plasmid was transformed into the evolved strains to generate the recombinant strains A-CodY-Lg-*gfp* and C-CodY-Lg-*gfp*. After two rounds of mutagenesis and flow cytometric screening, the fluorescence distribution of the cell populations shifted toward higher intensity in the second round, indicating enrichment of high-expression variants (Fig. 6b). Upon re-screening, the A10 mutant derived from the BS-MutaT7<sup>A</sup> system exhibited a 42.9 % increase in RFI, while the C4 mutant from the BS-MutaT7<sup>C</sup> system showed a 57.5 % increase (Fig. 6b). Sequencing analysis revealed that the *codY* gene in A10 carried an L245P mutation, along with mutations in the  $P_{43}$  promoter. The editable window spanned 1137 bp, with the most distal mutation introduced was located in the  $P_{43}$  promoter region, approximately 940 bp downstream of the T7 transcription start site. The C4 harbored V171I and D208N substitutions in CodY.

To validate the effect of *codY* mutations on  $\beta$ -Lg synthesis, the corresponding *codY* mutant expression cassettes were integrated into the genome of BSF01 to generate the recombinant strains A10-codY and C4-codY. These strains were then transformed with the pHT01- $P_{566}$ -lgb-*gfp* plasmid to generate A-codY-Lg and C-codY-Lg. Shake flask fermentation showed that the titers of  $\beta$ -Lg in A-codY-Lg and C-codY-Lg reached 0.43 g/L and 0.51 g/L, representing 16.2 % and 37.8 % increases over the strain BS- $P_{566}$ -Lg (Fig. 6c). These results demonstrate that the continuous evolution of the global transcriptional regulator CodY via the BS-MutaT7 system significantly enhances  $\beta$ -Lg expression in *B. subtilis*. To further evaluate production performance, fed-batch fermentation of strain C-codY-Lg was conducted in a 5-L fermenter (Fig. 6d). The culture reached a maximum OD<sub>600</sub> of approximately 170 at 48 h, and the  $\beta$ -Lg titer reached 3.92 g/L, with the productivity of 0.082 g/L/h.

#### 4. Conclusion

In this study, we developed a T7 RNA polymerase-guided continuous evolution system in *B. subtilis* (BS-MutaT7). As a well-characterized model organism and industrial workhorse, *B. subtilis* plays a central role in advancing research in protein expression and metabolic regulation. By constructing libraries containing different fusion protein linkers, we screened and identified optimal fusion configurations compatible with *B. subtilis*, enabling efficient and sustained mutagenesis. The optimal BS-MutaT7<sup>A</sup>, featuring TadA8e fused to T7RNAP without linker, achieved a target mutation rate of  $1.2 \times 10^{-5}$  s.p.b., representing a 7000-fold higher than the host genomic mutation rate. The optimal BS-MutaT7<sup>C</sup>, featuring PmCDA1 fused to T7RNAP via the (GGGGS)<sub>3</sub> linker and co-expressed with UGI, exhibited a mutation rate of  $5.8 \times 10^{-5}$  s.p.b., corresponding to a 37,000-fold increase. Both systems demonstrated high processivity, maintaining mutation rates of  $5.8 \times 10^{-6}$  s.p.b. and  $2.9 \times 10^{-5}$  s.p.b. within a 5 kb DNA region. Comparative analysis

showed that BS-MutaT7<sup>C</sup> achieved a higher mutation rate than BS-MutaT7<sup>A</sup>, indicating superior genome editing efficiency in *B. subtilis*. Functionally, BS-MutaT7<sup>A</sup> and BS-MutaT7<sup>C</sup> enhanced tigecycline resistance in *B. subtilis* by 16- and 12-fold, respectively. Moreover, the BS-MutaT7 system was applied to evolve the global transcriptional regulator CodY, leading to a  $\beta$ -Lg titer of up to 3.92 g/L. These outcomes underscored the effectiveness and stability of BS-MutaT7 as a platform for accelerated continuous directed evolution. To expand the mutational spectrum, we explored the fusion of dual deaminases to T7RNAP and the co-expression of TadA8e-T7RNAP and PmCDA1-T7RNAP on a single plasmid. However, both strategies resulted in suboptimal editing efficiency. Therefore, future research will focus on engineering multi-enzyme complex to enable the simultaneous introduction of an expanded mutation spectrum on the genome. In summary, by expanding the applicability of T7-guided mutagenesis systems to Gram-positive bacteria, BS-MutaT7 provides a robust and versatile platform for genome-scale evolution, accelerating the development of high-performance chassis cell and functional genetic elements.

#### CRedit authorship contribution statement

**Bin Wang:** Writing – original draft, Methodology, Investigation, Data curation. **Yaokang Wu:** Writing – review & editing. **Xueqin Lv:** Supervision. **Long Liu:** Supervision. **Jianghua Li:** Supervision. **Guocheng Du:** Supervision. **Jian Chen:** Project administration. **Yanfeng Liu:** Writing – review & editing, Validation, Supervision.

#### Declaration of competing interest

The authors declare that they have no known competing financial interests or personal relationships that could have appeared to influence the work reported in this paper.

#### Acknowledgements

This study was financially supported by the National Key Research and Development Program (2024YFF1106800), National Natural Science Foundation of China (32172349), the Foundation for Innovative Research Groups of the National Natural Science Foundation of China (32021005), the Jiangsu Basic Research Center for Synthetic Biology (BK20233003), and the Natural Science Foundation of Jiangsu Province (BK20202002).

#### Appendix A. Supplementary data

Supplementary data to this article can be found online at <https://doi.org/10.1016/j.synbio.2025.04.010>.

#### References

- [1] Brustad EM, Arnold FH. Optimizing non-natural protein function with directed evolution. *Curr Opin Chem Biol* 2011;15(2):201–10. <https://doi.org/10.1016/j.cbpa.2010.11.020>.
- [2] Packer MS, Liu DR. Methods for the directed evolution of proteins. *Nat Rev Genet* 2015;16(7):379–94. <https://doi.org/10.1038/nrg3927>.
- [3] Arnold FH. Directed evolution: bringing new chemistry to life. *Angew Chem Int Ed Engl* 2017;57(16):4143–8. <https://doi.org/10.1002/anie.201708408>.
- [4] Wang Y, Xue P, Cao M, Yu T, Lane ST, Zhao H. Directed evolution: methodologies and applications. *Chem Rev* 2021;121(20):12384–444. <https://doi.org/10.1021/acs.chemrev.1c00260>.
- [5] Sellés Vidal L, Isalan M, Heap JT, Ledesma-Amaro R. A primer to directed evolution: current methodologies and future directions. *RSC Chem Biol* 2023;4(4): 271–91. <https://doi.org/10.1039/d2cb00231k>.
- [6] Rix G, Liu CC. Systems for *in vivo* hypermutation: a quest for scale and depth in directed evolution. *Curr Opin Chem Biol* 2021;64:20–6. <https://doi.org/10.1016/j.cbpa.2021.02.008>.
- [7] Molina RS, Rix G, Mengiste AA, Alvarez B, Seo D, Chen H, et al. *In vivo* hypermutation and continuous evolution. *Nat Rev Methods Primers* 2022;2. <https://doi.org/10.1038/s43586-022-00130-w>.

- [8] Chu W, Guo Y, Wu Y, Lv X, Li J, Liu L, et al. Enhancing cellular and enzymatic properties through *in vivo* continuous evolution. *ChemBiochem* 2024;25(24). <https://doi.org/10.1002/cbic.202400564>.
- [9] Esvelt KM, Carlson JC, Liu DR. A system for the continuous directed evolution of biomolecules. *Nature* 2011;472(7344):499–503. <https://doi.org/10.1038/nature09929>.
- [10] Ravikumar A, Arzumanyan GA, Obadi MKA, Javanpour AA, Liu CC. Scalable, continuous evolution of genes at mutation rates above genomic error thresholds. *Cell* 2018;175(7):1946–1957.e13. <https://doi.org/10.1016/j.cell.2018.10.021>.
- [11] Tian R, Zhao R, Guo H, Yan K, Wang C, Lu C, et al. Engineered bacterial orthogonal DNA replication system for continuous evolution. *Nat Chem Biol* 2023;19(12):1504–12. <https://doi.org/10.1038/s41589-023-01387-2>.
- [12] Tian R, Rehm FBH, Czernecki D, Gu Y, Zurcher JF, Liu KC, Chin JW. Establishing a synthetic orthogonal replication system enables accelerated evolution in *E. coli*. *Science* 2024;383(6681):421–6. <https://doi.org/10.1126/science.adk1281>.
- [13] Halperin SO, Tou CJ, Wong EB, Modavi C, Schaffer DV, Dueber JE. CRISPR-guided DNA polymerases enable diversification of all nucleotides in a tunable window. *Nature* 2018;560(7717):248–52. <https://doi.org/10.1038/s41586-018-0384-8>.
- [14] Komor AC, Kim YB, Packer MS, Zuris JA, Liu DR. Programmable editing of a target base in genomic DNA without double-stranded DNA cleavage. *Nature* 2016;533(7603):420–4. <https://doi.org/10.1038/nature17946>.
- [15] Ma Y, Zhang J, Yin W, Zhang Z, Song Y, Chang X. Targeted AID-mediated mutagenesis (TAM) enables efficient genomic diversification in mammalian cells. *Nat Methods* 2016;13(12):1029–35. <https://doi.org/10.1038/nmeth.4027>.
- [16] Sakata RC, Ishiguro S, Mori H, Tanaka M, Tatsuno K, Ueda H, et al. Base editors for simultaneous introduction of C-to-T and A-to-G mutations. *Nat Biotechnol* 2020;38(7):865–9. <https://doi.org/10.1038/s41587-020-0509-0>.
- [17] Grünwald J, Zhou R, Lareau CA, Garcia SP, Iyer S, Miller BR, et al. A dual-deaminase CRISPR base editor enables concurrent adenine and cytosine editing. *Nat Biotechnol* 2020;38(7):861–4. <https://doi.org/10.1038/s41587-020-0535-y>.
- [18] Hao W, Cui W, Suo F, Han L, Cheng Z, Zhou Z. Construction and application of an efficient dual-base editing platform for *Bacillus subtilis* evolution employing programmable base conversion. *Chem Sci* 2022;13(48):14395–409. <https://doi.org/10.1039/d2sc05824c>.
- [19] Hao W, Cui W, Liu Z, Suo F, Wu Y, Han L, Zhou Z. A new-generation base editor with an expanded editing window for microbial cell evolution *in vivo* based on CRISPR–Cas12b engineering. *Adv Sci* 2024;11(22). <https://doi.org/10.1002/adv.202309767>.
- [20] Wu Y, Li Y, Liu Y, Xiu X, Liu J, Zhang L, et al. Multiplexed *in-situ* mutagenesis driven by a dCas12a-based dual-function base editor. *Nucleic Acids Res* 2024;52(8):4739–55. <https://doi.org/10.1093/nar/gkac228>.
- [21] Anzalone AV, Randolph PB, Davis JR, Sousa AA, Koblan LW, Levy JM, et al. Search-and-replace genome editing without double-strand breaks or donor DNA. *Nature* 2019;576(7785):149–57. <https://doi.org/10.1038/s41586-019-1711-4>.
- [22] Nelson JW, Randolph PB, Shen SP, Everette KA, Chen PJ, Anzalone AV, et al. Engineered pegRNAs improve prime editing efficiency. *Nat Biotechnol* 2021;40(3):402–10. <https://doi.org/10.1038/s41587-021-01039-7>.
- [23] Tabor S, Richardson CC. A bacteriophage T7 RNA polymerase/promoter system for controlled exclusive expression of specific genes. *Proc Natl Acad Sci U S A* 1985;82(4):1074–8. <https://doi.org/10.1073/pnas.82.4.1074>.
- [24] Seo D, Koh B, Eom G-e, Kim HW, Kim S. A dual gene-specific mutator system installs all transition mutations at similar frequencies *in vivo*. *Nucleic Acids Res* 2023;51(10). <https://doi.org/10.1093/nar/gkad266>. e59–e59.
- [25] Moore CL, Papa LJ, Shoulders MD. A processive protein chimera introduces mutations across defined DNA regions *in vivo*. *J Am Chem Soc* 2018;140(37):11560–4. <https://doi.org/10.1021/jacs.8b04001>.
- [26] Park H, Kim S. Gene-specific mutagenesis enables rapid continuous evolution of enzymes *in vivo*. *Nucleic Acids Res* 2021;49(6). <https://doi.org/10.1093/nar/gkaa1231>. e32–e32.
- [27] Álvarez B, Mencía M, de Lorenzo V, Fernández LÁ. *In vivo* diversification of target genomic sites using processive base deaminase fusions blocked by dCas9. *Nat Commun* 2020;11(1). <https://doi.org/10.1038/s41467-020-20230-z>.
- [28] Mengiste AA, Wilson RH, Weissman RF, Papa Iii LJ, Hendel SJ, Moore CL, et al. Expanded mutaT7 toolkit efficiently and simultaneously accesses all possible transition mutations in bacteria. *Nucleic Acids Res* 2023;51(6). <https://doi.org/10.1093/nar/gkad003>. e31–e31.
- [29] Mengiste AA, McDonald JL, Nguyen Tran MT, Plank AV, Wilson RH, Butty VL, Shoulders MD. MutaT7GDE: a single chimera for the targeted, balanced, efficient, and processive installation of all possible transition mutations *in vivo*. *ACS Synth Biol* 2024;13(9):2693–701. <https://doi.org/10.1021/acssynbio.4c00316>.
- [30] Cravens A, Jamil OK, Kong D, Sockolosky JT, Smolke CD. Polymerase-guided base editing enables *in vivo* mutagenesis and rapid protein engineering. *Nat Commun* 2021;12(1). <https://doi.org/10.1038/s41467-021-21876-z>.
- [31] Wang Q, You J, Li Y, Zhang J, Wang Y, Xu M, Rao Z. Continuous evolution of protein through T7 RNA polymerase-guided base editing in *Corynebacterium glutamicum*. *ACS Synth Biol* 2024;14(1):216–29. <https://doi.org/10.1021/acssynbio.4c00606>.
- [32] Butt H, Ramirez JLM, Mahfouz M. Synthetic evolution of herbicide resistance using a T7 RNAP-based random DNA base editor. *Life Sci Alliance* 2022;5(12). <https://doi.org/10.26508/lsa.202201538>.
- [33] Chen H, Liu S, Padula S, Lesman D, Griswold K, Lin A, et al. Efficient, continuous mutagenesis in human cells using a pseudo-random DNA editor. *Nat Biotechnol* 2019;38(2):165–8. <https://doi.org/10.1038/s41587-019-0331-8>.
- [34] Hao W, Cui W, Cheng Z, Han L, Suo F, Liu Z, et al. Development of a base editor for protein evolution via *in situ* mutation *in vivo*. *Nucleic Acids Res* 2021;49(16):9594–605. <https://doi.org/10.1093/nar/gkab673>.
- [35] Yan X, Yu HJ, Hong Q, Li SP. Cre/lox system and PCR-based genome engineering in *Bacillus subtilis*. *Appl Environ Microbiol* 2008;74(17):5556–62. <https://doi.org/10.1128/AEM.01156-08>.
- [36] Zhang XZ, Zhang YHP. Simple, fast and high-efficiency transformation system for directed evolution of cellulase in *Bacillus subtilis*. *Microb Biotechnol* 2010;4(1):98–105. <https://doi.org/10.1111/j.1751-7915.2010.00230.x>.
- [37] Wang B, Wu Y, Lv X, Liu L, Li J, Du G, et al. Synergistic regulation of chassis cell growth and screening of promoters, signal peptides and fusion protein linkers for enhanced recombinant protein expression in *Bacillus subtilis*. *Int J Biol Macromol* 2024;280(Pt 3):136037. <https://doi.org/10.1016/j.ijbiomac.2024.136037>.
- [38] Foster PL. Methods for determining spontaneous mutation rates. *Methods Enzymol* 2006;409:195–213. [https://doi.org/10.1016/S0076-6879\(05\)09012-9](https://doi.org/10.1016/S0076-6879(05)09012-9).
- [39] Radchenko EA, McGinty RJ, Aksenova AY, Neil AJ, Mirkinn SM. Quantitative analysis of the rates for repeat-mediated genome instability in a yeast experimental system. *Methods Mol Biol* 2018;1672:421–38. [https://doi.org/10.1007/978-1-4939-7306-4\\_29](https://doi.org/10.1007/978-1-4939-7306-4_29).
- [40] Maughan H, Galeano B, Nicholson WL. Novel *rpoB* mutations conferring rifampin resistance on *Bacillus subtilis*: global effects on growth, competence, sporulation, and germination. *J Bacteriol* 2004;186(8):2481–6. <https://doi.org/10.1128/JB.186.8.2481-2486.2004>.
- [41] Ponniah K, Loo TS, Edwards PJB, Pascal SM, Jameson GB, Norris GE. The production of soluble and correctly folded recombinant bovine  $\beta$ -lactoglobulin variants A and B in *Escherichia coli* for NMR studies. *Protein Expr Purif* 2010;70(2):283–9. <https://doi.org/10.1016/j.pep.2009.12.006>.
- [42] Loch JI, Bonarek P, Tworzydło M, Polít A, Hawro B, Łach A, et al. Engineered  $\beta$ -lactoglobulin produced in *E. coli*: purification, biophysical and structural characterisation. *Mol Biotechnol* 2016;58(10):605–18. <https://doi.org/10.1007/s12033-016-9960-z>.
- [43] Totsuka M, Katakura Y, Shimizu M, Kumagai I, Miura K, Kaminogawa S. Expression and secretion of bovine beta-lactoglobulin in *Saccharomyces cerevisiae*. *Agric Biol Chem* 1990;54(12):3111–6. <https://doi.org/10.1271/bbb1961.54.3111>.
- [44] Kalidas C, Joshi L, Batt C. Characterization of glycosylated variants of beta-lactoglobulin expressed in *Pichia pastoris*. *Protein Eng* 2001;14(3):201–7. <https://doi.org/10.1093/protein/14.3.201>.
- [45] Biermann L, Tadele LR, Benatto Perino EH, Nicholson R, Lilge L, Hausmann R. Recombinant production of bovine  $\alpha$ s1-casein in genome-reduced *Bacillus subtilis* strain IIG-Bs-20-5-1. *Microorganisms* 2025;13(1). <https://doi.org/10.3390/microorganisms13010060>.
- [46] Zhu Y, Sun P, Li C, Zhang Y, Wang Y, Li J, et al. Enhanced extracellular production of alpha-lactalbumin from *Bacillus subtilis* through signal peptide and promoter screening. *Food Sci Hum Wellness* 2024;13(4):2310–6. <https://doi.org/10.26599/fshw.2022.9250192>.
- [47] Westers L, Dijkstra DS, Westers H, van Dijk JM, Quax WJ. Secretion of functional human interleukin-3 from *Bacillus subtilis*. *J Biotechnol* 2006;123(2):211–24. <https://doi.org/10.1016/j.jbiotec.2005.11.007>.
- [48] Brinsmade SR, Alexander EL, Livny J, Stettner AI, Segre D, Rhee KY, Sonenshein AL. Hierarchical expression of genes controlled by the *Bacillus subtilis* global regulatory protein CodY. *Proc Natl Acad Sci U S A* 2014;111(22):8227–32. <https://doi.org/10.1073/pnas.1321308111>.
- [49] Cai D, Zhu J, Zhu S, Lu Y, Zhang B, Lu K, et al. Metabolic engineering of main transcription factors in carbon, nitrogen, and phosphorus metabolisms for enhanced production of bacitracin in *Bacillus licheniformis*. *ACS Synth Biol* 2019;8(4):866–75. <https://doi.org/10.1021/acssynbio.9b00005>.
- [50] Cao H, Villatoro-Hernandez J, Weme RDO, Frenzel E, Kuipers OP. Boosting heterologous protein production yield by adjusting global nitrogen and carbon metabolic regulatory networks in *Bacillus subtilis*. *Metab Eng* 2018;49:143–52. <https://doi.org/10.1016/j.ymben.2018.08.001>.
- [51] Cao H, Kuipers OP. Influence of global gene regulatory networks on single cell heterogeneity of green fluorescent protein production in *Bacillus subtilis*. *Microb Cell Fact* 2018;17(1):134. <https://doi.org/10.1186/s12934-018-0985-9>.
- [52] Huang Z, Zhang C, Chen S, Ye F, Xing XH. Active inclusion bodies of acid phosphatase PhoC: aggregation induced by GFP fusion and activities modulated by linker flexibility. *Microb Cell Fact* 2013;12:25. <https://doi.org/10.1186/1475-2859-12-25>.
- [53] García-Fruitós E, González-Montalbán N, Morell M, Vera A, Ferraz RM, Arís A, et al. Aggregation as bacterial inclusion bodies does not imply inactivation of enzymes and fluorescent proteins. *Microb Cell Fact* 2005;4(1). <https://doi.org/10.1186/1475-2859-4-27>.